Dominance of the Final State in Photoemission Mapping of the Fermi Surface of Co/Cu(001)

Xingyu Gao, Alexey N. Koveshnikov, Reginaldt H. Madjoe, Roger L. Stockbauer, and Richard L. Kurtz

Department of Physics and Astronomy, Louisiana State University, Baton Rouge, Louisiana 70803-4001

(Received 3 October 2002; published 24 January 2003)

The Fermi surface of tetragonally distorted fcc Co films grown on Cu(001) has been investigated with first-principles calculations and compared with an experimental determination using angle-resolved photoemission. The angular distributions for $h\nu = 21$–45 eV are dominated by the structure of the final states rather than by the shape of the Fermi surface. Theoretical estimates of the photoemission matrix elements support this observation. This suggests that photoemission can have limitations in mapping Fermi surfaces, especially for materials that exhibit flat, closely spaced valence bands.

DOI: 10.1103/PhysRevLett.90.037603 PACS numbers: 79.60.Dp, 71.20.Gj

The electronic structure of the Fermi surface (FS) determines many physical and chemical properties that are relevant in material and device design. In thin films, coupling of Fermi surface periodicities with quantum well states is known to both stabilize film thicknesses at characteristic values [1] as well as transmit spin-dependent information between layers. In giant magnetoresistance and in magnetic tunneling junctions employing this phenomena, spin-dependent scattering at the Fermi surface gives rise to enhanced magnetic sensitivity. In addition, investigations of the structure of the Fermi surface of cuprate superconductors have been instrumental in improving our understanding of those materials. For these reasons, it is important to develop and characterize new tools for extracting Fermi surfaces.

In these diverse materials, it is not always possible to apply a traditional de Haas–van Alphen measurement of the FS due to its need for pure, crystalline material with long scattering lengths. For this reason, Fermi surface mapping using angle-resolved ultraviolet photoelectron spectroscopy (ARPES) has become common. There have been many recent efforts using this method to study the $3d$ transition metals, superconductors, as well as other materials [2–6].

The implicit assumption in FS mapping is that the spectral weight in angle-resolved photoemission is dominated by the structure exhibited by the Fermi surface of the material. Actually, the photoemission process is an excitation from the initial state, the FS, to a final-state located $h\nu$ eV higher in energy. In this Letter, we show that photoemission from Co films grown on Cu(001) gives angular distributions that are dominated by the structure of the *final state* in the photoexcitation process, and the locus of intensity in k space *does not* resemble cross-sectional slices through the Fermi surface. First-principles calculations are used to predict these photoemission matrix elements, and they are found to agree reasonably well with the spectral weight found in the experimental data. This suggests that caution be used in interpreting Fermi surfaces mapped with photoemission and close coupling with a theoretical description is essential.

In the model of photoemission that is typically used to evaluate data, the final-state momentum of the detected free electron lies on a sphere with a k-space radius determined by its kinetic energy. It is coupled into the bulk excited state, essentially a time-reversed LEED state, via $k_{\|}$ conservation. $k_{\perp}$ is determined by using an approximation of a parabolic free-electron-like band in a constant inner potential V_0 [7]. This final state is essentially a slice through the Brillouin zone establishing the k values from where the excited electron can originate. The locus of points where this sphere intersects with the Fermi surface establishes the k values where photoemission intensity is expected. By changing the photon energy, the excited Fermi-level electrons change kinetic energy, and different initial (and final) k states within the Brillouin zone are sampled.

The matrix elements in the photoemission process reflect the overlap of the initial (occupied) states with the final (unoccupied) excited states, *and* the manner in which they couple to the detected photoelectron. The existence of a photoemission transition resulting in a detected electron means that there must be a coincidence of initial and final states at these points in k space, separated in energy by $h\nu$, and having symmetries that can couple through the momentum operator.

In the calculations below, we compute the photoemission matrix elements using realistic calculations of the final-state bands for all the potential k points that are sampled by the detected electron. In Cu, these calculations have been shown to give accurate predictions of the final bands in detailed comparisons with ARPES and VLEED measurements [8]. For the case of Co/Cu(001), we will find that the final state dominates the shape of the angular distribution of photoelectrons from the Fermi level, and not the Fermi contour itself. This effect can be especially significant for materials with flat bands near E_F such as $3d$ metals and superconductors and suggests that a close coupling between theory and experiment be maintained in interpreting such data.

To compute the photoemission angular distributions and their asymmetries, we have used WIEN97.9 [9,10] to perform a spin-polarized linearized augmented plane

wave first-principles calculation including spin-orbit interaction. In these calculations, the generalized gradient approximation was used to treat exchange and correlation and a basis set of 375 plane waves was used for each spin which includes additional local orbitals added to improve the quality of the empty final states [11]. The Co was assumed to have a bulk tetragonally distorted structure [12–14] with in-plane lattice parameters that of Cu (3.615 Å) and out-of-plane spacing that is compressed by 3.7% (3.42 Å). The Co was magnetized in-plane along the [100] direction.

Using an fcc structure without the tetragonal distortion, our own calculation of the Co band structure is essentially consistent with other calculations in the literature [15,16]. For the tetragonal distortion here, the main difference is that the bands with $\Delta_5^{\downarrow}$ and $\Delta_5^{\uparrow}$ character split into two inequivalent bands due to the reduced symmetry.

Figure 1 displays three-dimensional representations of the FS calculated for this bulk tetragonally distorted fcc Co. The top-left surface 1(a) is the single majority-spin $3d$-$4sp$ hybrid band centered at Γ with an open orbit at the L point. This band is very similar to the $3d$-$4sp$ hybrid Fermi surface in Cu, and has a strong contribution from majority $3d$ bands ($d_{z^2}^{\downarrow}$ and $d_{xy}^{\downarrow}$) at energies close to E_F, as mentioned in Ref. [17]. The other surfaces are three different minority-spin surfaces. In Fig. 1(b), the ellipsoidal hole pockets and the closed surface in Fig. 1(d) are primarily of d_{xy} and d_{xz+yz} symmetry. As is evident in Fig. 1(d), the tetragonal distortion induces an asymmetry in these states along the [001] direction in comparison with [100] or [010]. The minority-spin surface in Fig. 1(c) contains large open orbits and is primarily of $d_{x^2-y^2}$ and d_{z^2} character.

Figure 2 outlines the states probed in the photoemission experiment. The spheroidal arcs drawn in Fig. 2(a) show the region of the Brillouin zone (BZ) that is probed by photon energies of 21, 31, and 45 eV, respectively, using the FS of Fig. 1(d) as an example. If one looks down on these BZs from the top, one would see the initial (FS) and the final (excited) states' DOS as given in Figs. 2(b) and 2(c). Those figures include contributions from neighboring zones and those in 2(b) include contributions from all of the FS structures in Fig. 1. The calculated Fermi surface cross sections in Fig. 2(b) are given by the solid lines while the gray features give the density of states (DOS) within ± 0.25 eV of E_F. Since the dipole transition involves $\Delta\ell = \pm 1$, the contours shown in Fig. 2(c) give the corresponding p_z and p_{xy} excited states lying $h\nu$ in energy above E_F; there are no f levels there. It is the overlap of these states in 2(b) and 2(c) coupled with the momentum matrix operator that give rise to photoemission. In 2(c), note the narrow regions of k space that have an appreciable DOS.

The photoemission experiments were performed at Louisiana State University's Center for Advanced Microstructures and Devices (CAMD) synchrotron at the Plane Grating Monochromator (PGM) beam line [18]. Measurements of Fermi surfaces using photoemission can be accomplished in two manners. While varying the detection angle, spectra can be accumulated as a function of binding energy and, when a peak moves through E_F, a FS crossing is recorded. Alternately, data can be acquired by

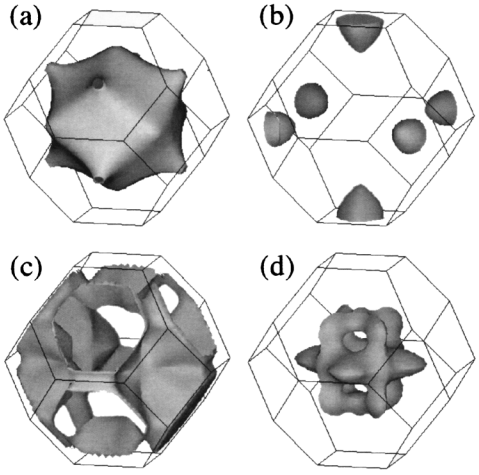

FIG. 1. Calculated Fermi surfaces of 3.7% tetragonally distorted (z-compressed) fcc Co. (a) spin-up with primarily $4sp$-like and (b)–(d) spin-down $3d$ Fermi surfaces.

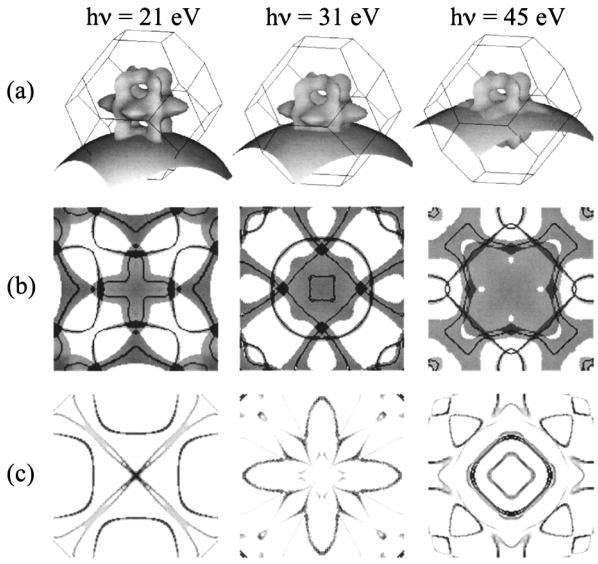

FIG. 2. Illustration of the region of the Brillouin zone sampled for three different photon energies $h\nu = 21$, 31, and 45 eV. The spherical slice intercepting the third spin-down Fermi surface is the free-electron final state that is detected in the experiment and its intersection with the Fermi surfaces gives the loci of k points sampled. (b) Density of states within ± 0.25 eVof E_F (the initial states in photoemission) and the solid black lines give the contours of E_F as they intercept the free-electron spheres in (a) above. (c) Density of states of the p final states at $h\nu \pm 0.25$ eV above E_F. The center of each panel in (b) and (c) is along the Γ-X line and the edge of each panel is ± 1.74 Å (corresponding to the Γ-X distance).

setting the spectrometer at E_F and measuring the spectral intensity while scanning the detection angle. In general, one assumes that the locus of points at which intense emission from the Fermi surface is observed describes the shape of the Fermi surface [19]. We used a two-dimensional display-type ellipsoidal-mirror analyzer to image the energy-resolved angular distributions of electrons ejected from surfaces [20].

The Cu substrate was prepared by cycles of Ar^+ sputtering at 1 keV and annealing to 700 K. Co films ($\sim$ 10 monolayers thick) were then grown at room temperature by electron bombardment of cobalt wire of high purity in a UHV chamber. Co films on Cu(001) are well known to grow in a pseudomorphic face-centered cubic structure compressed by 3.7% in the z direction [12–14]. The films were thick enough that the underlying Cu substrate was not observed in photoemission. In the present experiments, linear p-polarized light was incident on the sample at 45° and the angular distributions were collected in a 27° half angle about the sample normal and the energy resolution was $\sim$0.3 eV. More information about the details of the experimental setup can be found in Ref. [21].

In Fig. 3(a), images of the angular distribution of photoemission from the FS of a 10 monolayer (ML) Co/Cu(001) film are shown for photon energies of 21, 31, and 45 eV. The solid angles accepted in the images are scaled to provide a linear representation in k space and can be compared directly to the states in Fig. 2 and the predicted photoemission angular distributions in 3(b). Despite the fourfold symmetry of the film along the crystal's normal [001], both images exhibit a twofold emission pattern due to the polarization direction of the incident photon beam. Any top-bottom asymmetry is due to the slight misalignment of the crystal along a rotation axis normal to the film plane. In Fig. 3(a), the 21 eV image shows an intense x-like structure centered at the Γ-X axis with intensity along the [110] and [1$\bar{1}$0] directions, respectively. The 31 eV image, slicing the FS closer along the Γ-X direction, gives a pattern with two intense diagonal features, similar to the corner of a diamond, with a single more intense unresolved feature on the left. The 45 eV image is more complicated with the most intense features being two diagonals with several lower-intensity structures.

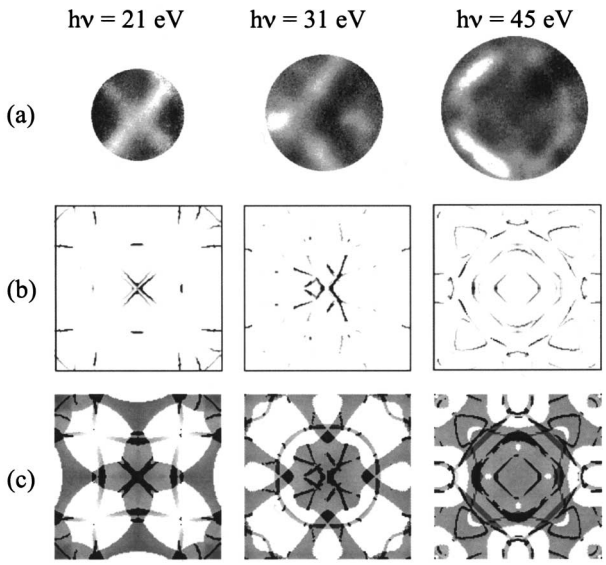

FIG. 3. Photoelectron angular distributions from the Fermi surface of 10 ML Co/Cu(001) for $h\nu = 21$, 31, and 45 eV measured with a display-type analyzer. (b) Calculated photoemission angular distributions corresponding to the initial states in 2(b) and the final states in 2(c) with the bounding box dimensions being ± 1.74 Å^{-1}. The data in (a) are scaled to match in Å^{-1}. In (c), we overlay the calculated angular distributions from (b) as black contours on top of the DOS within ± 0.25 eV of E_F from 2(b). These contours do *not* match the shape of this initial DOS; rather, they match the shapes of the *final states* 2(c).

From the calculated electronic band structure, it is possible to produce an estimate of the photoelectron angular distribution at given photon energies and this is shown in Fig. 3(b). This is accomplished by calculating the momentum matrix elements between the initial states (the FS) and the final states in the usual approximation of a slowly varying photon field [22]; the intensity is given by

$$\frac{d\sigma}{d\Omega} \propto |\mathbf{A} \cdot \langle \psi_i | \mathbf{P} | \psi_f \rangle|^2 \delta(E_f - E_i - h\nu).$$

The (complex) momentum matrix elements are obtained at the locations in the Brillouin zone given by the final-state electron's momentum, the arcs in Fig. 2(a). An inner potential of 13.4 eV (accounting for the work function) was used in the calculation and the results were rather insensitive to the specific choice (within ± 2 eV).

In Fig. 3(b), the predicted photoelectron angular distributions are shown using p-polarized light incident in the horizontal plane at an angle of 45° from the normal. This polarization choice (matching that of the experiment) is responsible for the left-right asymmetry in 3(b). In order to account for both k broadening and a nonzero experimental energy resolution, we have computed the matrix elements using a ± 0.25 eV energy width in both the initial and final states. This rather large energy width accommodates the limited number of k points in the calculation.

One can see from this figure that the essential aspects of the measured patterns are reproduced; the x-shaped feature for $h\nu = 21$ eV image is clearly seen and the scale in reciprocal space is close to that observed experimentally. For $h\nu = 31$ eV, the calculation also gives a reasonably good match. The two "arms" of intensity are seen directed towards the intense, unresolved lobe to the left. Even the feature directed at 11 o'clock from the top arm is visible in the experimental data. There is a lobe of intensity to the right that is not predicted in the calculation.

The $h\nu = 45$ eV data also shows a correspondence to the calculated data with square-shaped structures one within another and the polarization of the light making it most intense to the left. In this case, though, we expect departure from the better agreement observed at the lower photon energies due to the limited number of plane waves used which restricts the validity of the empty states in the 45 eV panel of Fig. 3(b). We expect that the addition of more local orbitals at energies exceeding 45 eV above E_F may provide better agreement with experiment.

In Fig. 3(c), we reproduce the density of states within ± 0.25 eV of E_F, from Fig. 2(b), and we overlay them with a thresholded copy of Fig. 3(b), where all points exhibiting a calculated photoemission matrix element is rendered black. Despite the good agreement of those calculations with the angle-resolved photoemission data, these matrix elements do not at all resemble the "shapes" of the Fermi surface *initial state* DOS. Especially when compared with the black contours of E_F in Fig. 2(b), the lack of correspondence between measured angular distribution and the initial state is clear. Finally, when the computed angular distributions in Fig. 3(b) are compared with the *final state* DOS of Fig. 2(c), one finds that the good agreement makes a compelling case that we are primarily observing the contours of the final state rather than the Fermi surface.

For all three photon energies, the initial state has a quite different shape from that seen in both the calculated and experimentally observed photoemission pattern. The initial state is quite broad in both E and $\mathbf{k}$ due to the small dispersion (or "flatness") of the bands at the Fermi level. The final state, on the other hand, disperses much more rapidly in $E(\mathbf{k})$. Since the photoemission spectral weight results as an overlap of these two states, coupled by the momentum matrix operator, the rapid dispersion of the final state provides the strongest influence in determining the locations in $\mathbf{k}$, where photoemission transitions occur. Consequently, the photoelectron angular distributions reflect the structure of that final state to a greater degree than the contours of the initial state, the Fermi surface.

This phenomenon is generally to be expected for materials with flat bands and we have observed similar strong final-state effects in ARPES from Ni films and from the $3d$ bands of bulk Cu. In the latter case, the d bands occur at higher binding energy, yet their angular distributions are also dominated by the final state. For Cu, the Fermi surface arises from sp-like states which disperse much more rapidly. This results in Cu FS photoemission angular distributions that exhibit the features of both the initial and final states.

In summary, we have used first-principles calculations to predict the angular distribution of photoelectrons from the Fermi level of Co/Cu(001), and we have compared them with experimental determinations. The predicted angular distributions agree with observations but the shapes of the angular distributions are found to reflect those of the final states rather than the initial occupied state, which in these measurements was the Fermi surface. In the case of Co and other flat-band materials, the lack of strong dispersion of the initial state means that the angular distribution will be more heavily influenced by the final state which disperses much more rapidly, and provides for significant matrix elements within much more limited regions of k space. This suggests that photoemission measurements of Fermi surfaces for flat-band materials such as heavy fermions and cuprate superconductors be coupled closely with theoretical descriptions to identify the origin of the observed angular distributions.

The authors thank D. Browne and R. Hall for helpful discussions, and R. Wendell, J. Toups, A. Acatrinei, and the staff of the CAMD synchrotron for their help during this work. This work was funded by NSF under Grant No. DMR-9802278.

[1] J. Ortega *et al.*, Phys. Rev. B **47**, 1540 (1993).
[2] D. H. Lu *et al.*, Phys. Rev. Lett. **86**, 4370 (2001).
[3] P. Aebi *et al.*, Phys. Rev. Lett. **76**, 1150 (1996).
[4] G. J. Mankey *et al.*, Phys. Rev. Lett. **78**, 1146 (1997).
[5] T. Greber, T. J. Kreutz, and J. Osterwalder, Phys. Rev. Lett. **79**, 4465 (1997).
[6] M. Hochstrasser *et al.*, Phys. Rev. B **60**, 17 030 (1999).
[7] F. J. Himpsel, Appl. Opt. **19**, 3964 (1980).
[8] V. N. Strocov *et al.*, Phys. Rev. Lett. **81**, 4943 (1998).
[9] P. Blaha, K. Schwarz, and S. T. Trickey, Comput. Phys. Commun. **59**, 399 (1990).
[10] P. Blaha, K. Schwarz, and J. Luitz, *WIEN97, A Full Potential Linearized Augmented Plan Wave Package for Calculating Crystal Properties*, edited by Karlheinz Schwarz (Technische Universität Wien, Austria, 1999).
[11] J. Perdew, K. Burke, and Y. Wang, Phys. Rev. B **54**, 16 533 (1996).
[12] A. Clarke *et al.*, Surf. Sci. **187**, 327 (1987).
[13] C. M. Schneider *et al.*, J. Phys. C **8**, 1657 (1988).
[14] H. Li and B. P. Tonner, Surf. Sci. **237**, 141 (1990).
[15] J. L. Pérez-Díaz and M. C. Muöz, Phys. Rev. B **52**, 2471 (1995).
[16] G. J. Mankey, R. F. Willis, and F. J. Himpsel, Phys. Rev. B **48**, 10 284 (1993).
[17] D. A. Papaconstantopoulous, *Handbook of the Band Structure of Elemental Solids* (Plenum, New York, 1985).
[18] R. L. Stockbauer *et al.*, Nucl. Instrum. Methods Phys. Res., Sect. A **291**, 505 (1990).
[19] P. Aebi *et al.*, Surf. Sci. **309**, 917 (1994).
[20] R. L. Kurtz *et al.*, Nucl. Instrum. Methods Phys. Res., Sect. A **319**, 257 (1992).
[21] X. Gao *et al.*, J. Appl. Phys. **91**, 7364 (2002).
[22] E. W. Plummer and W. Eberhardt, in *Advanced Chemical Physics*, edited by I. Prigogine and S. A. Rice (Wiley, New York, 1982), Vol. XLIX, p. 533.